Reversible Modulation of the Cr^{3+} Spin Dynamics in Colloidal $SrTiO_3$ Nanocrystals

William L. Harrigan and Kevin R. Kittilstved*

Department of Chemistry, University of Massachusetts Amherst, 710 N Pleasant St, Amherst, MA, 01003, USA

Supporting Information Placeholder

ABSTRACT: The spin relaxation dynamics of Cr^{3+} substitutional dopants in ~10-nm colloidal $SrTiO_3$ nanocrystals (NCs) has been studied by variable-temperature electron paramagnetic resonance (EPR) spectroscopy and continuous wave EPR power saturation measurements between 4.2 K and 50 K. The presence of self-trapped electrons introduced by anaerobic UV irradiation (photodoping) is able to effectively accelerate the spin relaxation dynamics of localized spins of Cr^{3+} through a cross-relaxation process. The extra electrons introduced during photodoping trap on Ti-sites creating Ti^{3+} defects with EPR transitions that are only observed at cryogenic temperatures due to fast spin-lattice relaxation. The change in the spin relaxation upon photodoping the Cr-doped $SrTiO_3$ NCs is totally reversible upon opening the sample to air. This result provides a novel strategy to modulate spin dynamics in individual NCs using photons where long-lived spins on dopant ions couple to the fast-relaxing spins from metastable, transient defects.

INTRODUCTION

Control over either the individual or collective behavior of spins in semiconductor nanomaterials is a grand challenge for the field of quantum information processing.[1-3] One class of materials that shows promise for this technology are the diluted magnetic semiconductors (DMSs) where a fraction of the diamagnetic cations of the host lattice are substituted with paramagnetic dopant ions. The exchange interaction between spatially-confined charge carriers such as excitons or conduction band electrons (e_{cb}^-) and paramagnetic centers in nanoscale DMSs has been exploited to produce new magneto-optical phenomena such as excitonic magnetic polarons.[4] However, traditional II-VI based DMS-QDs have isovalent dopants and do not possess appreciable n- or p-type carriers. The Fermi-level must therefore be modulated through incorporation of heterovalent dopants or reduction of the DMS-QD.

Previous work on colloidal semiconductor NCs demonstrated that electrons can be reversibly added to the conduction band by appropriate chemical reductants[5] or "photodoping" with UV photons in the presence of a sacrificial reductant under anaerobic conditions.[6-8] The introduction of chemically-stable e_{cb}^- into colloidal QDs by aliovalent doping has received increasing attention after the demonstrations of tunable localized surface plasmon resonances (LSPR) in Al^{3+}-doped ZnO (Al^{3+}:ZnO) QDs and Sn^{4+}:In_2O_3 NCs. Recently, the ability to modulate the carrier concentration of colloidal DMS-QDs has been shown to produce interesting effects in DMS-QDs including carrier-controlled magnetism[9] and spin dynamics,[10] and supercapacitance.[11]

We recently reported the synthesis and characterization of Cr^{3+}-doped $SrTiO_3$ colloidal NCs.[12] Through dopant-specific spectroscopic methods (including EPR, electronic absorption and emission), we confirmed that Cr^{3+} ions substitute at the Ti^{4+} site in the cuboidal NCs with ~10 nm edges. Herein, we present evidence that the spin dynamics of Cr^{3+} ions in colloidal $SrTiO_3$ NCs are extremely perturbed after photodoping, which does not produce e_{cb}^-, but localized Ti^{3+} defects. These "self-trapped electrons" at Ti^{3+} defects are confirmed by electronic absorption and continuous-wave (CW) electron paramagnetic resonance (EPR) spectroscopy and can be completely removed upon aerobic oxidation. The drastic change of the Cr^{3+} spin dynamics is evident even at room temperature by the disappearance of the Cr^{3+} EPR signal upon photodoping. We confirm the origin of this effect by performing EPR measurements as a function of temperature and power saturation rollover experiments between 4 K and 50 K. We invoke a cross-relaxation mechanism between localized Cr^{3+} and Ti^{3+} in photodoped $SrTiO_3$ to explain the EPR results. This study establishes a new type of dopant-defect interaction that is (1) enhanced by spatial confinement of charge carriers in NCs, and (2) unique to metal oxides with conduction band minima that are comprised of empty d orbitals (d^0 metal oxides such as TiO_2 and $SrTiO_3$).

RESULTS AND DISCUSSION

Figure 1 shows the electronic absorption spectra of $SrTiO_3$ and nominally 0.1% Cr:$SrTiO_3$ colloidal nanocrystal anaerobic suspensions in hexanes as a function of UV irradiation

time using a 75 W Xe lamp. The electronic absorption spectra of the as-prepared samples are dominated by the $SrTiO_3$ band gap transition above 3.2 eV. The Cr:$SrTiO_3$ NCs display a broad, weak transition that extends throughout the visible region and has been assigned in bulk Cr:$SrTiO_3$ as a metal-to-ligand charge transfer (MLCT) transition involving Cr^{3+} as the metal and the conduction band (empty Ti^{4+} 3d orbitals) as the ligand.[13] With increasing photodoping time, the spectra change and the physical appearance of the NCs change from transparent or light yellow to dark blue. This change in color is accompanied by a new feature in the electronic absorption spectrum centered at ~1.4 eV (~900 nm). This feature has been observed previously in reduced titanium oxides[14-16] and photodoped colloidal TiO_2 nanoparticles.[17-20] This new transition originates from the excitation of trapped electrons at Ti^{3+} centers to the $SrTiO_3$ conduction band (also known as a metal-to-metal charge transfer transition, MMCT). Similar to photodoped TiO_2, the near-IR transition does not shift in energy with increasing photodoping time, but does increase in optical density.

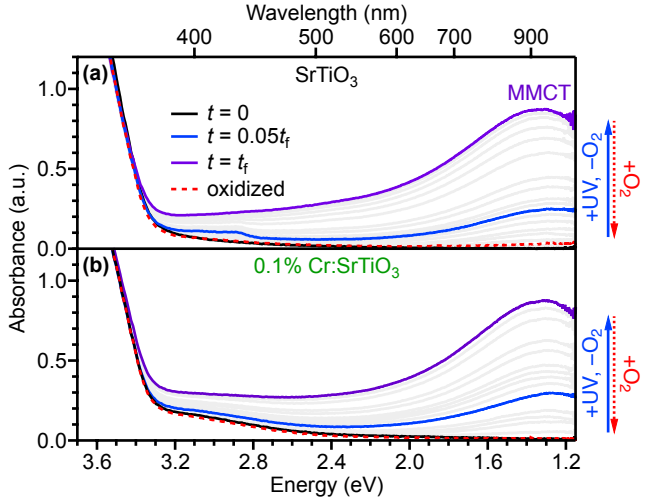

Figure 1. Electronic absorption spectra of air-free (a) $SrTiO_3$ and (b) 0.1% Cr:$SrTiO_3$ suspensions in hexane collected after different UV irradiation times. The spectra collected before irradiation (black line), and after irradiation at $0.05t_f$ (blue line) and t_f (purple line) are highlighted by colors. The spectra taken after reopening the cuvette to air is also shown (dashed red line). The t_f is arbitrarily defined as the time needed for the MMCT transition to reach an optical density equal to 0.87.

In pristine $SrTiO_3$, a weak, broad feature appears at 430 nm after short photodoping times (see Figure 1a), but disappears or becomes occluded by the intense MMCT transition that grows in at longer photodoping times. A similar visible absorption feature has been observed and assigned to transitions from the valence band to oxygen vacancies (V_O) in bulk $SrTiO_3$.[21-22] Notably, this feature is not observed for the Cr:$SrTiO_3$ NCs after similar photodoping times likely due to the stronger MLCT transition. We also looked in the mid-IR region, but photodoping does not appear to produce LSPRs such as those recently been reported for Nb-doped TiO_2 (see SI).[23] In addition, the band edge absorption does not shift with photodoping that further supports the self-trapping model for the electron and not as a delocalized e^-_{cb}, which should display a significant blue-shift of the band edge according to the Moss-Burstein effect if electrons accumulate in the conduction band.[23] Figure 1 shows that photodoping ultimately creates localized Ti^{3+} defects in both NCs that are consistent with previous studies on TiO_2 nanoparticles.[17-18,24] These electronic structure changes are also totally reversed upon reoxidizing the samples with air as shown in Figure 1.

The Cr^{3+}-centered d-d transitions are too weak to be observed in the spectra shown in Figure 1b. We therefore utilized EPR spectroscopy to confirm that Cr is trivalent and also monitor any changes in the Cr^{3+} signal upon introduction of Ti^{3+} defects in the Cr:$SrTiO_3$ NCs. EPR spectra were collected under the following conditions: (1) Cr:$SrTiO_3$ NCs before and after photodoping at room temperature, (2) Cr:$SrTiO_3$ and $SrTiO_3$ NCs after photodoping as a function of sample temperature and (3) microwave power at low temperatures.

The EPR spectra and color photographs of the colloidal Cr:$SrTiO_3$ NCs before and after photodoping at room temperature are shown in Figure 2. As previously reported,[12,25] Cr^{3+} in $SrTiO_3$ exhibits an isotropic EPR signal at $g = 1.978$ (B_o ~347 mT in Figure 2) which is consistent with substitutional doping of Cr^{3+} in the octahedral Ti^{4+} site of $SrTiO_3$. This signal corresponds to spin-allowed EPR transitions within the $^4A_2$ ground state of Cr^{3+}. The expected 4-line hyperfine pattern from $^{53}Cr^{3+}$ ions (relative abundance, rel. ab. = 9.5% with a nuclear spin of $I = 3/2$) is occluded by the inhomogeneously broadened central transition of the nuclear-spin free $^{52}Cr^{3+}$ isotopes (rel. ab. = ~84%). After photodoping, however, the Cr^{3+} EPR signal disappears completely at room temperature and the solution appears blue due to the MMCT transition shown in Figure 1 and in the color photograph in Figure 2. Both the color of the sample and the Cr^{3+} EPR signal reverts quantitatively to its original intensity upon reopening the sample to air. In addition, upon reoxidation a new feature at ~343 mT (g ~2.009) is clearly observed that we attribute to the reaction of Ti^{3+} with molecular O_2 to regenerate Ti^{4+} and form superoxide ions (O_2^-) at the NC surface. We recently observed this same defect-related signal in nominally undoped $SrTiO_3$ NCs that were prepared in the absence of hydrazine.[12]

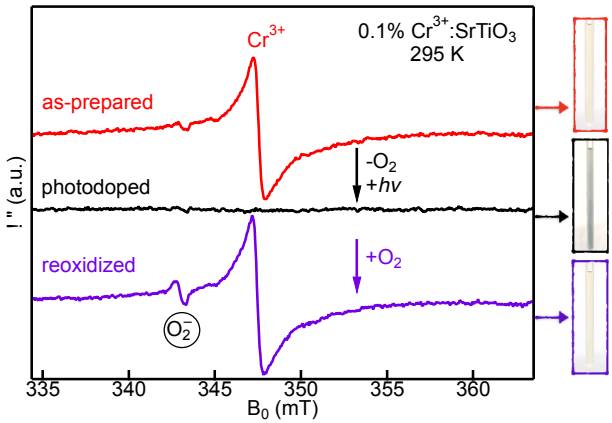

Figure 2. Room-temperature EPR spectra of 0.1% Cr:$SrTiO_3$ NCs in hexanes before (red) and after anaerobic photodoping (black), and after reoxidation (purple). Corresponding color photographs of representative Cr:$SrTiO_3$ samples in EPR tubes is included to the right of each EPR spectra.

The disappearance of the Cr^{3+} EPR signal in photodoped 0.1% Cr:$SrTiO_3$ could be explained by (1) the formation of a new EPR-silent Cr^{3+}-defect complex, (2) a change in the Cr^{3+} oxidation state, or (3) a possible interaction between Cr^{3+} and the paramagnetic Ti^{3+} defects, which typically requires low temperatures to observe by EPR due to fast spin-lattice relaxation dynamics. To evaluate which scenario was likely operative in the photodoped Cr:$SrTiO_3$ NCs, we measured EPR spectra at various temperatures down to 4.2 K. The EPR spectra of photodoped Cr:$SrTiO_3$ at various temperatures down to 77 K and photodoped $SrTiO_3$ at 4.2 K are shown in Figure 3. In the photodoped Cr:$SrTiO_3$ sample, we see the appearance of two broad signals that increase in intensity with decreasing temperature. The main feature is observed at ~347 mT (g = 1.978) and assigned to substitutional Cr^{3+} (see Figure 2), while the second signal at ~355 mT (g = ~1.95) is asymmetric and is assigned to self-trapped electrons located at Ti^{3+} defects.[26] This assignment of the Ti^{3+} signal is confirmed by the 4.2 K spectrum of photodoped $SrTiO_3$ also shown in Figure 3. Upon warming the photodoped Cr:$SrTiO_3$ to room temperature, we note the reappearance of a minor EPR signal from Cr^{3+} that we attribute to a small amount of air that was introduced through the low-pressure valve on the EPR tube during the thermal cycling.

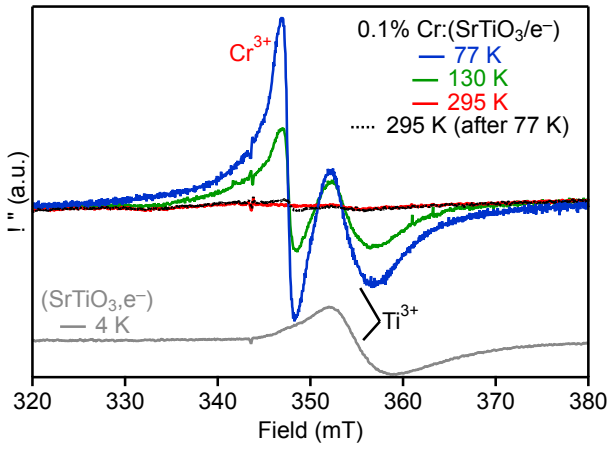

Figure 3. Variable-temperature EPR spectra collected on photodoped 0.1% Cr:$SrTiO_3$ NCs and 4.2 K spectrum of photodoped $SrTiO_3$ NCs. The spectra for photodoped Cr:$SrTiO_3$ were collected first at 295 K (red), and then decreased to 130 K (green) and 77 K (blue) followed by warming the sample again to 295 K (black dotted).

The behavior of the Cr^{3+} EPR signal in the photodoped Cr:$SrTiO_3$ NCs at various temperatures supports scenario 3 discussed above where the localized spins of Cr^{3+} are strongly interact with Ti^{3+} defects. We performed power saturation rollover studies with various microwave powers on Cr:$SrTiO_3$ NCs before and after photodoping, and photodoped Cr:$SrTiO_3$ NCs to confirm the effect of Ti^{3+} on the Cr^{3+} spin dynamics. Representative CW-EPR spectra of these three samples at various microwave powers and 4.2 K are shown in Figure 4. The EPR intensity for Cr^{3+} in the as-prepared Cr:$SrTiO_3$ sample and Ti^{3+} in the photodoped $SrTiO_3$ NCs is defined as ΔY, which is taken as the difference in the positive and negative χ" values. For the overlapping Cr^{3+} and Ti^{3+} EPR signals in the photodoped Cr:$SrTiO_3$ NCs, we define the EPR intensity by the maximum positive χ" and maximum negative χ" values, respectively. The Cr^{3+} EPR signal in the Cr:$SrTiO_3$ NCs before photodoping increases to a maximum peak intensity at ~8 mW before decreasing and broadening at higher powers. In contrast, the EPR signal of Ti^{3+} in photodoped $SrTiO_3$ NCs steadily increases without saturating even >200 mW. The EPR signals for both Cr^{3+} and Ti^{3+} in the photodoped Cr:$SrTiO_3$ NCs display behavior similar to the Ti^{3+} defects in photodoped $SrTiO_3$ NCs; continuously increasing without saturating with increasing microwave power. These spectra confirm that the spin dynamics of the Cr^{3+} dopants are efficiently modulated by the presence of Ti^{3+} defects.

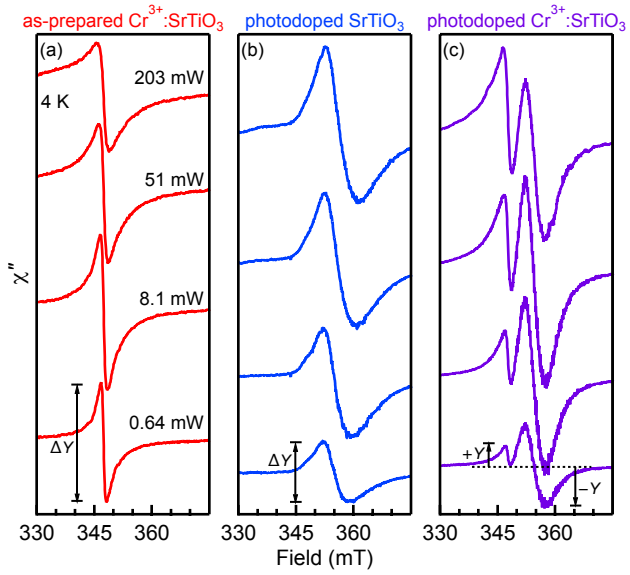

Figure 4. Representative CW-EPR spectra of (a) as-prepared Cr:$SrTiO_3$, (b) photodoped $SrTiO_3$, and (c) photodoped Cr:$SrTiO_3$ NCs at 4.2 K (frozen suspension) and selected microwave powers. Definitions for the signal intensities for the

different EPR-active species in the different sets of spectra are included graphically in the panels.

The EPR signal intensities (ΔY or |Y|) at 4.2 K of the Cr^{3+} or Ti^{3+} ions in the different samples in Figure 4 are plotted as a function of microwave power (h_1, converted to Gauss units) in Figure 5. For Cr:$SrTiO_3$ NCs before photodoping, the Cr^{3+} intensity exhibits typical saturation and rollover behavior; increasing steadily with increasing power until saturating at h_1 ~0.06 G and then decreasing with increasing h_1. The temperature dependence of this saturation behavior for the Cr^{3+} signal in Cr:$SrTiO_3$ NCs before photodoping shows a steady increase in the saturation power with increasing temperature (see SI). However, the peak intensities of Ti^{3+} in photodoped $SrTiO_3$ and Ti^{3+} and Cr^{3+} in photodoped Cr:$SrTiO_3$ both increase with increasing microwave power, but do not saturate even at 4.2 K.

The data in Figure 5 were used to estimate the magnitude of the total spin dynamics according to eq 1.

$$\Delta Y \text{ or } |Y| = c \cdot h_1 \left(1 + \frac{(h_1)^2}{P_2}\right)^{-\varepsilon} \quad (1a)$$

$$P_2 = (\gamma_e^2 T_1 \cdot T_2)^{-1} \quad (1b)$$

where c is a scaler and ε is a measure of line homogeneity. P_2 is proportional to the product of the spin-lattice and spin-spin relaxation rates ($1/T_1$ and $1/T_2$, respectively), and γ_e is the electron gyromagnetic ratio (see eq 1b).

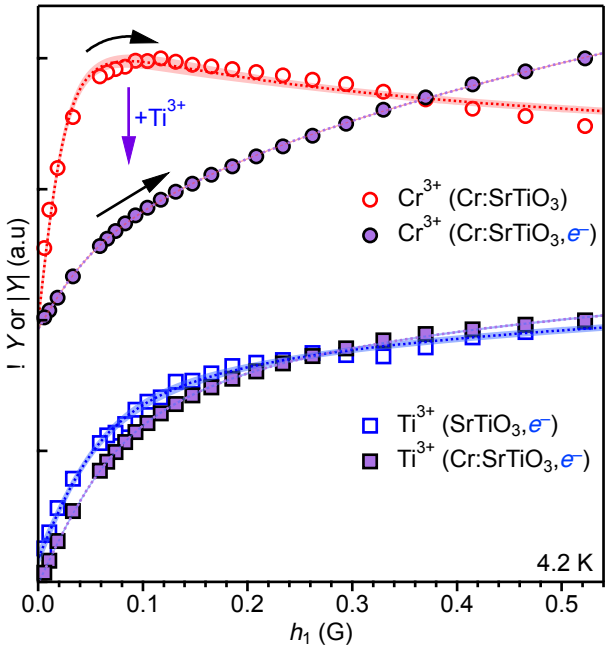

Figure 5. (a) Normalized CW-EPR intensities (ΔY or $|Y|$) as a function of incident microwave power (h_1) at 4.2 K for Cr^{3+} (red) and Ti^{3+} (blue) EPR signals in the following samples: Cr^{3+} in as-prepared Cr:$SrTiO_3$ (empty circles), Ti^{3+} in photodoped $SrTiO_3$ (empty squares), and the Cr^{3+} and Ti^{3+} signals in photodoped Cr:$SrTiO_3$ (filled circles and squares, respectively). The dashed curves through the data points are best fits to eq 1a (shaded regions are error bars on the fits).

The values of P_2 obtained from the experimental fits to the power-dependence of the EPR intensities are plotted as a function of temperature in Figure 6. The relaxation dynamics of the Cr^{3+} spins increase by at least a factor of two below 50 K when Ti^{3+} defects are also present in the NC. In addition, the Ti^{3+} relaxation dynamics show an even larger increase in the photodoped $SrTiO_3$ NCs when Cr^{3+} is present. This latter result could be caused by the relative distributions of Cr^{3+} dopants and Ti^{3+} defects in the ensemble of $SrTiO_3$ NCs. Furthermore, the density, speciation, and proximity of Ti^{3+} defects to surfaces, other Ti^{3+} centers and Cr^{3+} dopants is largely unknown.

While there is variability in the temperature dependence of the spin relaxation, the trend is consistent with regards to temperature and relaxation rates: (1) the relaxation rate is slowest for Cr^{3+} in $SrTiO_3$ NCs before photodoping and increases upon photodoping; and (2) the Ti^{3+} relaxation rate increases with the presence of Cr^{3+}.

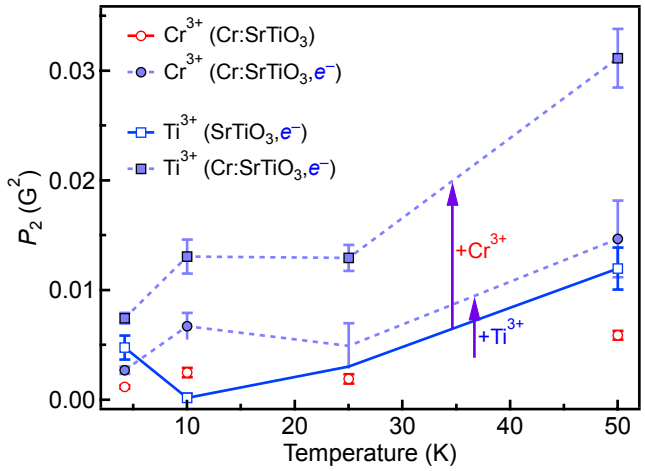

Figure 6. Temperature dependence of P_2, for Cr^{3+} (circles) and Ti^{3+} (squares) in before (open) and after (filled) photodoping either Cr:$SrTiO_3$ or $SrTiO_3$ NCs. Both signals have an increase in the spin dynamics overall relaxation rates increase when Ti^{3+} is present in the lattice. Lines are guides to the eye.

Systematic studies of spin relaxation rates of isovalent Cr^{3+} and Ti^{3+} in Al_2O_3 date back to the early 1960s.[27-28] Prokhorov first demonstrated that the spin-lattice relaxation times of $(Al_{1-x}M_x)_2O_3$ differ by many orders of magnitude at cryogenic temperatures for M = Cr^{3+} or Ti^{3+}. Spin-lattice relaxation times at 4.2 K for Cr:Al_2O_3 is ~50 ms, whereas for Ti:Al_2O_3 T_1 = ~0.1 ms.[27] These reported times are also sensitive to temperature and dopant concentration (self or resonant cross-relaxation).[28] Here, the difference in P_2 between Cr^{3+} in Cr:$SrTiO_3$ NCs and Ti^{3+} in photodoped $SrTiO_3$ NCs is much smaller than in Al_2O_3. This deviation is possibly due to the polaronic nature[29-30] of the self-trapped electron of Ti^{3+} in $SrTiO_3$ versus the localized $3d^1$ Ti^{3+} ion in Al_2O_3. Studies to address the effect of the Cr^{3+}:Ti^{3+} ratio on the spin relaxation dynamics are currently underway.

In the absence of pulsed EPR measurements to directly determine relaxation rates, we estimated T_2 by analysis of the EPR linewidth. The EPR spectra of Cr^{3+} in Cr:$SrTiO_3$ before photodoping at 4.2 K and microwave powers well below saturation were fit to the first-derivative of a pseudo-Voigt line profile (linear combination of a Lorentzian and Gaussian function). For Cr^{3+} in Cr:$SrTiO_3$ before photodoping, the Lorentzian linewidth is found to be Γ_L = 6.4 G (see SI), which equates to $T_2 \approx 18$ ns by the relation,[31] $T_2 = 2/(\gamma_e \Gamma_L)$. This value of T_2 at 4.2 K is similar to reported values for Cr^{3+} in bulk Al_2O_3.[32] Using eq 1b and the experimental P_2 value, $T_1 \approx 150$ μs. A strong concentration-dependence results in a range of T_1 values between 170 μs and 110 ms for Cr^{3+} in bulk Al_2O_3 at 4.2 K.[32-33] A similar study of the concentration dependence of T_1 has not been performed for Cr^{3+} in bulk $SrTiO_3$, but for a Cr concentration of 0.05% the value at 4.2 K is $T_1 \approx$ 1-5 ms.[34] The faster spin-lattice relaxation of the Cr^{3+} dopants in $SrTiO_3$ NCs before photodoping could arise from heterogeneity in dopant location and proximity to NC surfaces.[35]

Unfortunately, accurate deconvolution of the linewidths for the photodoped Cr:$SrTiO_3$ samples were complicated due to the overlapping signals of Cr^{3+} and Ti^{3+}. If we assume that the T_2 value of Cr^{3+} is unchanged after photodoping, then we estimate an accelerated $T_1 \approx 70$ μs for the Cr^{3+} dopants in photodoped Cr:$SrTiO_3$ NCs at 4.2 K. Prior studies of cross-relaxation in Cr^{3+},Ti^{3+} codoped Al_2O_3 have similar reductions in T_1-values of the Cr^{3+} dopants at low temperatures when Ti^{3+} is present.[28]

Previously, some of us demonstrated the introduction of Ti^{3+} defects could also be achieved in bulk Cr^{3+}-doped $SrTiO_3$ (and related Sr_2TiO_4) powders using $NaBH_4$.[36-37] After this chemical reduction, the Cr^{3+} concentration increases by an order of magnitude according to quantitative EPR measurements due to the *reduction* of EPR-silent Cr species to Cr^{3+} prior to formation of Ti^{3+} defects. No such increase in the Cr^{3+} EPR signal is observed at the start of photodoping (see SI). In addition, the EPR linewidth of Cr^{3+} significantly broadens after lattice Ti^{3+} defects are formed. We tentatively attributed this broadening to a magnetic interaction between Cr^{3+} and Ti^{3+}, however, we were limited due to inhomogeneous distributions of Ti^{3+} and V_O in the bulk material. This clear interaction in the current study suggests that similar broadening through cross-relaxation is also active in the reduced Cr:$SrTiO_3$, but the Ti^{3+} defects are limited to the (sub-)surface layers of the bulk powders.

CONCLUSIONS

We report the efficient and reversible modulation of the spin relaxation of Cr^{3+} dopants in colloidal $SrTiO_3$ NCs. This spin phenomenon results in the disappearance of the Cr^{3+} EPR signal at room temperature and can reappear either by (1) reoxidizing the Ti^{3+} defects in the NCs with air, or (2) lowering the sample temperature. The latter scenario also confirms the presence of paramagnetic Ti^{3+} defects. Power saturation rollover experiments at 4.2 K confirms the origin of the accelerated spin relaxation of Cr^{3+} in photodoped Cr:$SrTiO_3$ to an efficient, near-resonant, cross-relaxation involving Ti^{3+} defects.

While similar cross-relaxation processes are evident between the Cr^{3+} and Ti^{3+} defects these $SrTiO_3$ NCs and similar bulk lattices, these changes are quantitatively reversible by using only UV photons and mild oxidants. The facile generation of many Ti^{3+} defects within a single $SrTiO_3$ NC via photodoping ensures that every Cr^{3+} dopant is in spatial proximity for near-resonant cross-relaxation processes to dominate the Cr^{3+} spin dynamics even at room temperature. This discovery introduces an interesting spin-based phenomenon in colloidal semiconductor NCs. We are currently investigating the generality of cross-relaxation to other EPR-active isovalent and heterovalent dopants in $SrTiO_3$.

ASSOCIATED CONTENT

Supporting Information.
The Supporting Information is available free of charge on the ACS Publications website.
Additional experimental methods, details, and characterization (PDF)

AUTHOR INFORMATION

Corresponding Author

*E-mail: kittilstved@chem.umass.edu (K.R.K)

ORCID(ID)

Kevin R. Kittilstved: 0000-0002-9852-7454

Author Contributions

The manuscript was written through contributions of all authors.

Notes

No competing financial interests have been declared.

ACKNOWLEDGMENT

This work was supported by the National Science Foundation (DMR-1747593).

REFERENCES

(1) Berezovsky, J.; Mikkelsen, M. H.; Stoltz, N. G.; Coldren, L. A.; Awschalom, D. D. Picosecond coherent optical manipulation of a single electron spin in a quantum dot. *Science* **2008**, *320*, 349-352.

(2) Imamo$\bar{g}$lu, A.; Awschalom, D. D.; Burkard, G.; DiVincenzo, D. P.; Loss, D.; Sherwin, M.; Small, A. Quantum information processing using quantum dot spins and cavity QED. *Phys. Rev. Lett.* **1999**, *83*, 4204-4207.

(3) Clark, S. M.; Fu, K. M.; Ladd, T. D.; Yamamoto, Y. Quantum computers based on electron spins controlled by ultrafast off-resonant single optical pulses. *Phys. Rev. Lett.* **2007**, *99*, 040501.

(4) Beaulac, R.; Schneider, L.; Archer, P. I.; Bacher, G.; Gamelin, D. R. Light-induced spontaneous magnetization in doped colloidal quantum dots. *Science* **2009**, *325*, 973-976.

(5) Shim, M.; Guyot-Sionnest, P. n-Type colloidal semiconductor nanocrystals. *Nature* **2000**, *407*, 981-983.

(6) Liu, W. K.; Whitaker, K. M.; Kittilstved, K. R.; Gamelin, D. R. Stable photogenerated carriers in magnetic semiconductor nanocrystals. *J. Am. Chem. Soc.* **2006**, *128*, 3910-3911.

(7) Schimpf, A. M.; Gunthardt, C. E.; Rinehart, J. D.; Mayer, J. M.; Gamelin, D. R. Controlling carrier densities in photochemically reduced colloidal ZnO nanocrystals: size dependence and role of the hole quencher. *J. Am. Chem. Soc.* **2013**, *135*, 16569-16577.

(8) Schimpf, A. M.; Thakkar, N.; Gunthardt, C. E.; Masiello, D. J.; Gamelin, D. R. Charge-tunable quantum plasmons in colloidal semiconductor nanocrystals. *ACS Nano* **2014**, *8*, 1065-1072.

(9) Ochsenbein, S. T.; Feng, Y.; Whitaker, K. M.; Badaeva, E.; Liu, W. K.; Li, X. S.; Gamelin, D. R. Charge-controlled magnetism in colloidal doped semiconductor nanocrystals. *Nat. Nanotechnol.* **2009**, *4*, 681-687.

(10) Schimpf, A. M.; Rinehart, J. D.; Ochsenbein, S. T.; Gamelin, D. R. Charge-state control of Mn^{2+} spin relaxation dynamics in colloidal n-type $Zn_{1-x}Mn_xO$ nanocrystals. *J. Phys. Chem. Lett.* **2015**, *6*, 1748-1753.

(11) Brozek, C. K.; Zhou, D. M.; Liu, H. B.; Li, X. S.; Kittilstved, K. R.; Gamelin, D. R. Soluble supercapacitors: large and reversible charge storage in colloidal iron-doped ZnO nanocrystals. *Nano Lett.* **2018**, *18*, 3297-3302.

(12) Harrigan, W. L.; Michaud, S. E.; Lehuta, K. A.; Kittilstved, K. R. Tunable electronic structure and surface defects in chromium-doped colloidal $SrTiO_{3-\delta}$ nanocrystals. *Chem. Mater.* **2016**, *28*, 430-433.

(13) Blasse, G.; de Korte, P. H. M.; Mackor, A. The colouration of titanates by transition-metal ions in view of solar energy applications. *J. Inorg. Nucl. Chem.* **1981**, *43*, 1499-1503.

(14) Zuo, F.; Wang, L.; Wu, T.; Zhang, Z.; Borchardt, D.; Feng, P. Self-doped Ti^{3+} enhanced photocatalyst for hydrogen production under visible light. *J. Am. Chem. Soc.* **2010**, *132*, 11856-11857.

(15) Tan, H.; Zhao, Z.; Zhu, W. B.; Coker, E. N.; Li, B.; Zheng, M.; Yu, W.; Fan, H.; Sun, Z. Oxygen vacancy enhanced photocatalytic activity of perovskite $SrTiO_3$. *ACS Appl. Mater. Interfaces* **2014**, *6*, 19184-19190.

(16) Khomenko, V. M.; Langer, K.; Rager, H.; Fett, A. Electronic absorption by Ti^{3+} ions and electron delocalization in synthetic blue rutile. *Phys. Chem. Miner.* **1998**, *25*, 338-346.

(17) Schrauben, J. N.; Hayoun, R.; Valdez, C. N.; Braten, M.; Fridley, L.; Mayer, J. M. Titanium and zinc oxide nanoparticles are proton-coupled electron transfer agents. *Science* **2012**, *336*, 1298-1301.

(18) Kölle, U.; Moser, J.; Grätzel, M. Dynamics of interfacial charge-transfer reactions in semiconductor dispersions. Reduction of cobaltoceniumdicarboxylate in colloidal titania. *Inorg. Chem.* **1985**, *24*, 2253-2258.

(19) Bahnemann, D.; Henglein, A.; Lilie, J.; Spanhel, L. Flash photolysis observation of the absorption spectra of trapped positive holes and electrons in colloidal titanium dioxide. *J. Phys. Chem.* **1984**, *88*, 709-711.

(20) Henglein, A. Colloidal TiO_2 catalyzed photo- and radiation chemical processes in aqueous solution. *Bunsen-Ges. Phys. Chem., Ber.* **1982**, *86*, 241-246.

(21) Mitra, C.; Lin, C.; Robertson, J.; Demkov, A. A. Electronic structure of oxygen vacancies in $SrTiO_3$ and $LaAlO_3$. *Phys. Rev. B* **2012**, *86*, 155105.

(22) Rice, W. D.; Ambwani, P.; Bombeck, M.; Thompson, J. D.; Haugstad, G.; Leighton, C.; Crooker, S. A. Persistent optically induced magnetism in oxygen-deficient strontium titanate. *Nat. Mater.* **2014**, *13*, 481-487.

(23) De Trizio, L.; Buonsanti, R.; Schimpf, A. M.; Llordes, A.; Gamelin, D. R.; Simonutti, R.; Milliron, D. J. Nb-doped colloidal TiO_2 nanocrystals with tunable infrared absorption. *Chem. Mater.* **2013**, *25*, 3383-3390.

(24) Peper, J. L.; Vinyard, D. J.; Brudvig, G. W.; Mayer, J. M. Slow equilibration between spectroscopically distinct trap states in reduced TiO_2 nanoparticles. *J. Am. Chem. Soc.* **2017**, *139*, 2868-2871.

(25) Müller, K. A. In *Proceedings of the First International Conference on Paramagnetic Resonance*; Low, W., Ed.; Academic Press: New York, 1963; Vol. I, pp 17-43.

(26) Howe, R. F.; Grätzel, M. EPR observation of trapped electrons in colloidal titanium dioxide. *J. Phys. Chem.* **1985**, *89*, 4495-4499.

(27) Manenkov, A. A.; Prokhorov, A. M. Spin-lattice relaxation and cross-relaxation interactions in chromium corundum. *Sov. Phys. J. Exp. Theor. Phys.* **1962**, *15*, 54-59.

(28) Nisida, Y. Spin-lattice relaxation of Cr^{3+} in coexistence with Ti^{3+} in Al_2O_3. *J. Phys. Soc. Jpn.* **1965**, *20*, 1390-1399.

(29) Janotti, A.; Franchini, C.; Varley, J. B.; Kresse, G.; Van de Walle, C. G. Dual behavior of excess electrons in rutile TiO_2. *Phys. Status Solidi RRL* **2013**, *7*, 199-203.

(30) Hao, X.; Wang, Z.; Schmid, M.; Diebold, U.; Franchini, C. Coexistence of trapped and free excess electrons in $SrTiO_3$. *Phys. Rev. B* **2015**, *91*, 085204.

(31) Whitaker, K. M.; Ochsenbein, S. T.; Smith, A. L.; Echodu, D. C.; Robinson, B. H.; Gamelin, D. R. Hyperfine coupling in colloidal n-type ZnO quantum dots: effects on electron spin relaxation. *J. Phys. Chem. C* **2010**, *114*, 14467-14472.

(32) Manenkov, A. A.; Prokhorov, A. M. Spin-lattice relaxation in chromium corundum. *Sov. Phys. J. Exp. Theor. Phys.* **1960**, *11*, 527-530.

(33) Mims, W. B.; McGee, J. D. Cross relaxation in ruby. *Phys. Rev.* **1960**, *119*, 1233-1237.

(34) Azamat, D. V.; Dejneka, A.; Lancok, J.; Trepakov, V. A.; Jastrabik, L.; Badalyan, A. G. Pulse-electron paramagnetic resonance of Cr^{3+} centers in $SrTiO_3$. *J. Appl. Phys.* **2013**, *113*, 174106.

(35) Schimpf, A. M.; Ochsenbein, S. T.; Gamelin, D. R. Surface contributions to Mn^{2+} spin dynamics in colloidal doped quantum dots. *J. Phys. Chem. Lett.* **2015**, *6*, 457-463.

(36) Lehuta, K. A.; Kittilstved, K. R. Reversible control of the chromium valence in chemically reduced Cr-doped $SrTiO_3$ bulk powders. *Dalton. Trans.* **2016**, *45*, 10034-10041.

(37) Lehuta, K. A.; Haldar, A.; Zhou, D.; Kittilstved, K. R. Spectroscopic study of the reversible chemical reduction and reoxidation of substitutional Cr ions in Sr_2TiO_4. *Inorg. Chem.* **2017**, *56*, 9177-9184.

SYNOPSIS TOC

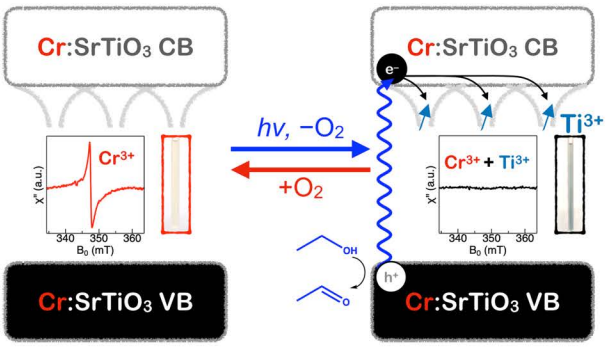

Author biography:

Kevin Kittilstved was born in Spokane, WA and graduated with degrees in chemistry from Gonzaga University (BS 2001) and the University of Washington (PhD 2006). He held postdoctoral positions at the Université de Genève (2006-2009) and the University of Washington (2010) prior to joining the University of Massachusetts Amherst as an Assistant Professor in January 2011 in the Department of Chemistry. Kevin is the recipient of the NSF CAREER Award and was recently promoted to Associate Professor with tenure. His research program focuses on understanding and exploiting the defect chemistry of inorganic materials to control physical properties from molecular nanoclusters to bulk powders.